Biochimica et Biophysica Acta 1850 (2015) 845–856

Contents lists available at ScienceDirect

Biochimica et Biophysica Acta

journal homepage: www.elsevier.com/locate/bbagen

A simple, fast and cost-effective method of synthesis of cupric oxide nanoparticle with promising antibacterial potency: Unraveling the biological and chemical modes of action

Ruchira Chakraborty [a], Raj Kumar Sarkar [b], Arijit Kumar Chatterjee [a], Unnikrishnan Manju [c], Asoke Prasun Chattopadhyay [b], Tarakdas Basu [a,*]

[a] Department of Biochemistry and Biophysics, University of Kalyani, Kalyani 741 235, West Bengal, India
[b] Department of Chemistry, University of Kalyani, India
[c] Materials Characterization Division, CSIR — Central Glass and Ceramic Research Institute, Kolkata 700032, West Bengal, India

ARTICLE INFO

Article history:
Received 4 August 2014
Received in revised form 19 January 2015
Accepted 21 January 2015
Available online 29 January 2015

Keywords:
Cupric oxide nanoparticle
Colloidal suspension
Antibacterial action
ROS generation
Modification of Cu(II) oxide NP
Growth media organics

ABSTRACT

Background: Gradual attainment of bacterial resistance to antibiotics led us to develop a robust method of synthesis of stable, colloidal cupric oxide nanoparticle of physiological pH with potential antibacterial action.
Methods: Cu(II) oxide NP was synthesized by reduction–oxidation of $CuCl_2$, using polyvinyl alcohol as stabilizer. Characteristics and antibacterial activity of the particles were investigated by techniques like UV–Vis spectrophotometry, DLS, AFM, TEM, EDS, FTIR, AAS, agar plating, FACS, gel electrophoresis and XPS.
Results: The NPs were about 50 nm in size and cubic in shape with two surface plasmon peaks at 266 and 370 nm and had semi-conducting behavior with a band gap of 3.40 and 3.96 eV. About 80% of precursor $CuCl_2$ was converted to NP. The minimum inhibitory and the minimum bactericidal concentrations of CuO-NP were respectively 120 and 160 μg/mL for *Escherichia coli* and 180 and 195 μg/mL for *Staphylococcus aureus* in Luria–Bertani medium. In growth media, the NPs got modified by media organics with displacement of the stabilizer PVA molecules. This modified NP (around 240 nm) killed cells by generating ROS, which finally caused membrane lipid per-oxidation and chromosomal DNA degradation in NP-treated cells.
Conclusion: Reports indicate that we are among the few who had prepared CuO-NP in colloidal form. The antibacterial potency of our particle in growth media was much promising than other reports. Our findings demonstrated that 'particle-specific' effect, not 'ion-specific' one, was responsible for the NP action.
General significance: The NP may be used as a sterilizing agent in various bioprocesses and as substituent of antibiotics, after thorough toxicological study.

© 2015 Elsevier B.V. All rights reserved.

1. Introduction

Increasing resistance in bacteria towards antibiotics makes it imperative to research on new nanodrugs to combat a wide spectrum of infectious diseases. From this standpoint, metallic and metal oxide nanoparticles may be potential agents, from which antimicrobial drugs can be designed in the future. Of the different metals, copper is recognized as a good and less expensive antimicrobial agent and there is an age-old tradition of Indians to preserve drinking water in copper vessels for sterility, even before the existence of microorganism was acknowledged. Some recent reports on antimicrobial potency of metallic copper and copper oxide nanoparticles [1–8] suggest that the NPs may have wide applications in developing antibacterial drugs and in sterilizing foods, liquids, medical instruments and implants, human tissues, textiles, public areas etc. Compared to bulk copper salts, NPs of metallic copper or copper oxides are believed to have an enhanced antimicrobial activity because of their large surface to volume ratio and crystallographic surface structure.

Cupric oxide NP was prepared, mostly in precipitated solid form, by different methods like solid state reaction [9], electrochemical method [10], sonochemical process [11], microwave irradiation [12] and sol–gel technique [13], with various morphological structures such as nanoparticles, nanowires, nanotubes, nanorods, nanoflakes, nanosheets, nanoneedles, nanoribbons, nanorings, nanoleaves and nanoflowers. However, the method of synthesis of CuO-NPs in a suspended colloidal form is very rare and so far our knowledge goes, there are only two published reports on the preparation of colloidal CuO-NP [14,15]. The present study deals with the i) synthesis of stable colloidal suspension of Cu(II) oxide NP of physiological pH-7.5 by an innovative method, which was simple, fast and economic compared to the above referred methods, ii) characterization of the size, shape,

* Corresponding author.
E-mail address: tarakdb@yahoo.com (T. Basu).

http://dx.doi.org/10.1016/j.bbagen.2015.01.015
0304-4165/© 2015 Elsevier B.V. All rights reserved.

composition and intrinsic properties (like optical and electrical) of the particles, iii) antibacterial potency and the biological mechanism of bacterial cell killing by the NPs and iv) chemical mechanism of the antibacterial action of CuO-NP.

2. Experimental

2.1. Preparation of Cu(II) oxide NP

Our method of synthesis of Cu(II) oxide NP was based on successive reduction–oxidation of $CuCl_2$ to CuO in presence of polyvinyl alcohol (PVA) and sodium borohydride ($NaBH_4$) under ambient condition. A solution of 5% PVA in Milli-Q water was first prepared by vigorous stirring for 2–3 h, until white foam was formed. To 3.0 mL of freshly prepared PVA, 1.5 mL of 100 mM $CuCl_2$ and 1.5 mL of Milli-Q water were added and vigorously stirred for about 2 h. Reduction of $CuCl_2$ to copper was first carried out by drop-wise addition of 9.0 mL of 33.72 mM $NaBH_4$ and pH of the reaction mixture was subsequently adjusted to 7.5 by adding 100 μl of 1(N) NaOH. Thereafter, the reduced copper was left for simple aerial oxidation by continuous stirring at 45 °C for 1–2 h, until a clear leafy green color appeared with the formation of CuO-NPs. Finally, pH of the solution was further adjusted to 7.5 with addition of 1–2 drops of 1.0(N) NaOH. The prepared colloidal suspension of Cu(II) oxide NP was stable for at least 2–3 months.

2.2. Characterization of the nanoparticles

2.2.1. Study of the optical property of the NP

The light absorption nature of the synthesized CuO-NP was investigated by scanning the absorbance of the 10 times diluted NP suspension in the wavelength region of 220–800 nm, using a UV–Vis spectrophotometer (Shimadzu, UV-1800); a solution of 10 times diluted 10 mM $CuCl_2$ in 1% PVA was taken in the reference cuvette.

2.2.2. Study of the size, shape and crystallinity of the NP

Hydrodynamic size of the NPs was regularly measured by a dynamic light scattering (DLS) instrument (Malvern, Nano-ZS). Moreover, to visualize the shape and to measure the size of core particles, the techniques of atomic force microscopy (AFM) and transmission electron microscopy (TEM) were used. For AFM study, dried NP film was prepared on a cleaned cover slip as described in [4] and scanned by an atomic force microscope (Veeco, di-Innova) in contact mode. For TEM study, NP suspension was placed on carbon-coated copper grid, dried in a vacuum desiccator, and analyzed by a transmission electron microscope (JEOL, JEM-2010) to obtain the size, shape and crystal planes [determined from the SAED (small angle electron diffraction) pattern] of the NPs.

2.2.3. Study of the composition of the NP and the trace of metal oxide bond in it

To analyze the elemental composition of CuO-NP, the NP suspension was taken on a cover-slip and dried in a vacuum desiccator. The cover-slip was then mounted using a carbon tape and the sample was coated with gold–paladium to study by an electron dispersion spectrometer (QUANTA-200).

Existence of metal oxide bond in Cu(II) oxide NP was traced by Fourier transformed infrared (FTIR) spectrometric study. NP suspension was first centrifuged at 55,000 rpm for 25 min in an ultracentrifuge machine (Sorvall, WX Ultra 90); the pellet was washed twice by Milli-Q water and then lyophilized in a lyophilizer (Heto, DW-3) to obtain fine dust of NPs, which was finally analyzed by a FTIR spectrometer (PerkinElmer L 120-000A), as described in [16].

2.2.4. Study of the conducting property of the NP

To investigate whether our CuO-NP had any conductive property, AFM study was performed using conductive probe-tip. NP sample was prepared on a silicon wafer and vacuum dried. The conductive mode AFM image was generated by measuring the current passing through the tip and the sample, when a DC bias was applied between them, using 'DLPCA-200 variable-gain, low-noise current amplifier' made by Femto, Germany.

2.2.5. Study of the extent of conversion of the precursor $CuCl_2$ to Cu(II) oxide NPs

The percentage of conversion of precursor $CuCl_2$ to Cu(II) oxide NP was determined by atomic absorption spectrometric (AAS) technique. For this study, the NP suspension was centrifuged at 55,000 rpm for 25 min; the supernatant was separated and the NP pellet was re-suspended in the same volume of Milli-Q water. The supernatant and the NP suspension (each of 1.0 mL) were acid digested and the copper content in each digested sample was analyzed using an atomic absorption spectrometer (PerkinElmer-AA200), as described in [4].

2.3. Analysis of antibacterial activity of CuO-NPs

This study was performed on Gram negative bacteria *Escherichia coli* K12 and Gram-positive bacteria *Staphylococcus aureus* 29213. For each bacterium, all the experiments were carried out with synchronized cells. The synchronization was done by the following steps: i) an inoculum of overnight grown cells was diluted 100 times in fresh Luria–Bertani (LB) medium [1.0 g bactotryptone, 0.5 g yeast extract and 1.0 g NaCl dissolved in 100 mL distilled water; pH adjusted to 7.5], ii) the inoculated cells were grown further at 37 °C in a gyratory shaker (Lab Companion, IS-971R) at 125 rpm, till the bacterial $(OD)_{600\ nm}$ reached the value 0.2 (corresponding to the exponentially grown cell concentration 10^8 cells/mL), iii) cells were then centrifuged, washed with and finally suspended in the same volume of starvation buffer (SB) [5.0 g KCl, 1.0 g NaCl, 1.2 g Tris, 0.1 g $MgSO_4$, 1.0 mL of 1.0 M $CaCl_2$ in 1000 mL distilled water; pH adjusted to 8.1], and iv) the cells were allowed to starve with shaking at 37 °C for 1 h for synchronization.

2.3.1. Study of the antibacterial potency of the NP

The strength of antibacterial action of CuO-NP was studied by determining its minimum inhibitory concentration (MIC) and the minimum bactericidal concentration (MBC) on *E. coli* and *S. aureus* cells. For a particular bacterium, the MIC of an antibacterial agent is defined as such a concentration, which when present in growth medium causes complete inhibition of cell growth without cell killing even after overnight (18 h) incubation [8]. On the other hand, the MBC of an antimicrobial substance is defined as the concentration, the presence of which in the growth medium results 99.9% cell killing on overnight (18 h) incubation [8]. The following protocol was used to determine the MIC and MBC of Cu(II) oxide NP. Synchronized cells, made as described above, were diluted 100 times in fresh LB medium containing different concentrations of the NP ranging from 0 to 160 μg/mL (in terms of copper content, considering 80% conversion of $CuCl_2$ to CuO-NP, as observed from the AAS result). The diluted cultures were incubated at 37 °C with shaking at 125 rpm for 18 h. Cell aliquots of equal amount were withdrawn from each of the incubated cultures and each aliquot was serially diluted in SB. An amount of 0.1 mL cells from properly diluted samples was spread on LB agar plates [1.5% w/v agar in LB medium] with a glass-spreader and the plates were kept upside down in an incubator at 37 °C, until the colonies appeared. Viable cell counts were calculated by multiplying the number of colonies with the dilution factor. The culture that showed no change in the number of viable cells before and after incubation had contained the NP at MIC, and the culture which showed the number of viable cells after incubation to be 0.1% of that before incubation had contained the NP at MBC.

2.3.2. Study of the generation of reactive oxygen species (ROS) in the NP-treated bacterial cells

The extent of ROS production in bacterial cells was estimated by using 2′, 7′-dichlorodihydrofluorescein diacetate ($DCFH_2$-DA) as a visual indicator. The principle of the assay is that $DCFH_2$-DA can easily cross cell membrane and is hydrolyzed to $DCFH_2$ by cellular esterase; oxidation of $DCFH_2$ by intracellular ROS produces highly fluorescent DCF [6]. In this study, synchronized cells of *E. coli* K12 were diluted 100 times in fresh LB medium containing sub-MIC level of NP (90 μg/mL) and were subsequently allowed to shake at 37 °C for 18 h. The cells were then washed with and finally suspended in saline (8.0 g/L NaCl and 0.2 g/L KCl); the suspended cells were then incubated in dark for 2 h with 10 μM $DCFH_2$-DA prior to measurement of ROS, using a flow cytometer (Becton Dickinson, FACSCalibur). Fluorescence was collected in the green channel (FL-1H, 530/30 nm) of the flow-cytometer equipped with an argon laser (488 nm) and with standard filter set-up. The data were represented by scattered plot of side scatter vs. green fluorescence intensity and were analyzed using 'cell quest' software (Becton and Dickinson).

2.3.3. Study of the occurrence of lipid per-oxidation in the NP-exposed cell membrane

The extent of lipid peroxidation of cell membrane was estimated by thiobarbituric acid (TBA) assay utilizing spectrophotometric technique [17]. The principle of the assay was that during per-oxidation of lipids, the oxidation of polyunsaturated fatty acids produce malonaldehyde (MDA), which reacts with TBA producing a chromophore with absorption maximum at 532 nm. Therefore, the level of chromophoric absorption intensity at 532 nm was a quantitative measure of lipid per-oxidation. For this study, synchronized cells were exposed to two different concentrations (90 and 120 μg/mL) of the NP in LB medium for 18 h, as described in the preceding Section 2.3.2. 1.0 mL of NP-exposed culture was centrifuged and the cell pellet was suspended in 100 μL of SDBME buffer [4.5 mg Tris–HCl, 2.66 mg Tris base, 30 μl 10% SDS, 200 μL 1 M DTT and 770 μL H_2O] and heated for 5 min in a boiling water bath for cell lysis. An aliquot of 100 μL of cell extract was mixed with 200 μL of TBA–trichloroacetic acid (TCA)–hydrochloric acid (HCl) reagent (15% TCA and 0.375% TBA dissolved in 0.25 NHCl) and heated for another 15 min in boiling water bath. After cooling, the flocculent precipitates were removed by centrifugation at 12,000 rpm for 10 min. The absorbance of the supernatant was measured at 532 nm in a UV–Vis spectrophotometer (Shimadzu, UV1800), to estimate the level of lipid per-oxidation according to:

$$\text{LPO activity} = \frac{\text{absorbance} \times \text{total volume}}{\text{reaction} \times \text{sample volume} \times \text{molar extinction coeff.} \times \text{protein concentration} \times \text{nM/mg/unit.}}$$

The protein concentration in the cell lysate was assayed by the standard Bradford method [18] and the value of molar extinction coefficient of the chromophore was known to be $1.56 \times 10^5\ \text{Mol}^{-1}\ \text{cm}^{-1}$ [17].

2.3.4. Study of the DNA degradation in the NP-treated bacterial cells

The event of DNA degradation was investigated by isolating the chromosomal DNA from the CuO-NP-treated cells and further employing agarose gel electrophoresis with it. DNA was isolated according to the method of Wilson [19] and the gel electrophoresis study was performed according to the method of Sambrook and Rusell [20]. Here, synchronized cells were treated with 120 μg/mL (MIC) and 135 μg/mL (a concentration in between MIC and MBC) Cu(II) oxide NP in LB for 18 h and the genomic DNA was isolated from such cells. The DNA was electrophoresed in 1% (w/v) agarose gel for 1 h, using Tris-acetate-EDTA buffer.

2.3.5. Study of the interaction of the NP with media organics and amino acids

UV–Vis spectrophotometric study was performed to investigate whether there was any interaction between NP with media organics, by scanning the absorption profile of the growth medium LB in the wavelength region (450–800) nm with stepwise addition of CuO-NP [by 30 μg/mL in each step, up to the concentration of 180 μg/mL (above MBC for *E. coli*)]. In vitro interaction of the NP with the L-amino acids was also studied by scanning the absorption profile of the NP (of concentration 360 μg/mL) in the wavelength region (220–600) nm with stepwise addition (0, 10, 25, 50, 75, 100, 200 and 500 μg/mL) of single amino acids (viz., basic amino acid — Lys, acidic amino acid — Glu, polar amino acid — Ser and non-polar amino acid — Gly) as well as the mixture of all the 20 different L- amino acids, mixed in the proportion as present in the MOPS medium [21].

2.3.6. Study of the modification of the NP

To understand the mechanism of CuO-NP action i.e., whether there was any modification of NPs through interaction with the components of growth medium, X-ray photoelectron spectroscopic (XPS) study was performed on the NP-amino acid interaction. For XPS study, films of the NPs alone and of the modified NPs by lysine were made on cover slips, as was done in the case of AFM study. Experiment was carried out in a PHI-5000 VersaProbe II Scanning XPS Microprobe using monochromatic Al Kα radiations at room temperature. More details on the experimental set up are available in [22].

3. Results and discussion

In this study, we synthesized colloidal form of cupric oxide NP in an innovative way, which was simple, cheap and fast. In our method of synthesis, the primary precursor molecule $CuCl_2$ was subjected to successive reduction–oxidation processes under ambient condition, in the presence of $NaBH_4$ as the reducing agent and PVA as the stabilizing agent. A recent report mentioned the use of $NaBH_4$ and PVA in the synthesis of metallic copper NP [23]. In our method, 1 N NaOH was added extra so that the reduction–oxidation reaction of $CuCl_2$ to CuO-NP, through the intermediate formation of metallic copper, could take place at slightly basic pH 7.5. The pH-7.5 being the physiological pH also, our method of synthesis of CuO-NP was, therefore, a novel one from the aspect of the study of its role on any biological system viz., bacteria. It should be mentioned here that with increase of pH above 7.5, the reaction rate increased gradually (as observed from the gradual decrease of aerial oxidation period) and consequently the synthesized CuO particles, before being properly stabilized, agglomerated to precipitate down. Moreover, our method was rare in the sense that it produced Cu(II) oxide NP in the suspended colloidal form; in most reported methods, CuO-NPs were synthesized in solid precipitated form [9–13]. Literature review shows that there were only two reports on the synthesis of colloidal cupric oxide NP [14,15].

The color of our NP-suspension was deep green (Fig. 1A, inset), indicating that the NPs were of CuO (not Cu_2O) because, a) similar feature was observed in the case of the colloidal CuO-NP prepared by Son et al. [14] and b) the color of Cu_2O-NPs was reported to be red in nature [24,25].

3.1. Characterization of the synthesized CuO-NPs

3.1.1. Absorbance, size, shape and crystallinity of the NPs

UV-Visible spectrum of the NP suspension displayed two absorption peaks, a large sharp one at 266 nm and a small shallow one at 370 nm (Fig. 1A). Such two-peaked spectra were obtained in the cases of rose- and shuttle-like structures of CuO-NP [26,27], whereas in most other cases a single peak appeared within the range of 325 to 380 nm [3,12, 28,29]. For metal oxide nanoparticles, spectral peak was due to the surface plasmon resonance, caused by collective oscillations of

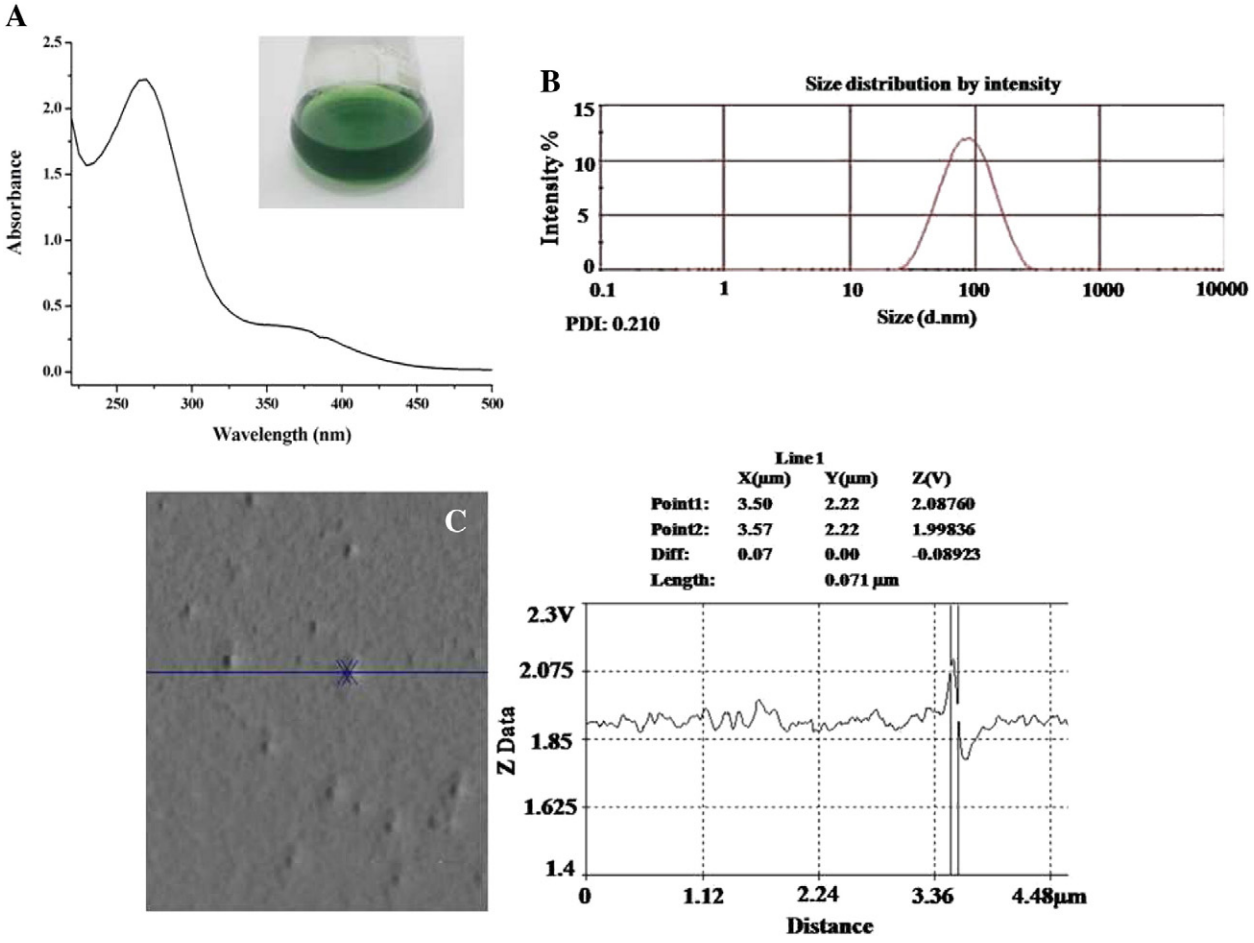

Fig. 1. Absorbance and size of CuO-NPs. A) UV–Vis spectrum of CuO-NP, inset showed the dark green color of the NPs; B) pattern of size distribution of the NPs measured by particle size analyzer; C) AFM image of CuO-NPs and scanned parameter of the arrow-marked particle.

free conduction band electrons, when excited by incident light of wavelength that far exceeded the size of the particles. The appearance of two peaks was suggested to be due to shape-induced absorption, employing discrete dipole approximation theory [27]. The cubic shape of our CuO-NPs, as observed from the TEM image (Fig. 2), might be responsible for the existence of 266 nm plasmon peak, similar to that in cases of rose- and shuttle-like nanoparticles of CuO [26,27]. Stability of the NPs at ambient condition was monitored by observing the nature of the plasmon spectrum after every 15 days. Hardly any difference in the intensity of spectrum was observed up to about 3 months, which indicated that highly stable Cu(II) oxide NPs were prepared by our method. Loss of stability of the NPs above 3 months was evident from the appearance of green precipitate at the bottom of the NP-container with decrease in intensity of the overall spectrum.

The mean size of the NPs, measured by DLS instrument, was found to be about (80 ± 20) nm with a PDI (poly dispersity index) value

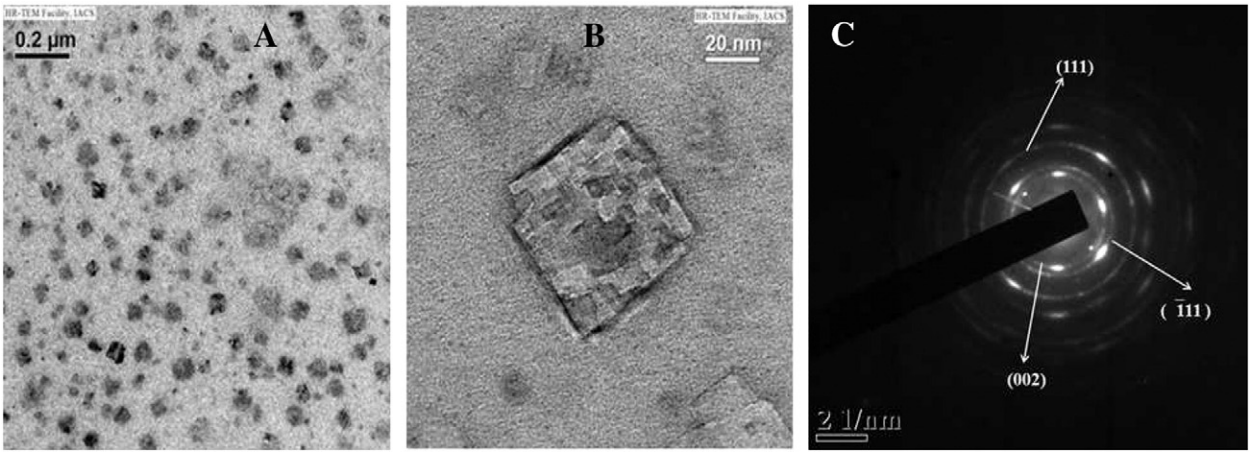

Fig. 2. TEM images of CuO-NP. A) Number of particles in a field of view; B) 10 times magnified image of a single particle in the field; C) SAED pattern of CuO-NP.

of around 0.2 (Fig. 1B). The value of the PDI signified good quality (homogeneous) sample preparation. However, the DLS instrument principally measures the hydrodynamic size, which is always somewhat larger than the real size of core particle. Actual size of the particles was, therefore, measured by both AFM and TEM. Fig. 1C shows the AFM image of the NPs in a field of view, where all the particles appear to be of equal size; AFM-determined size of the particles was around 70 nm. The TEM image of almost equal-sized particles in a field of view is shown in Fig. 2A. Fig. 2B represents the 10 times magnified image of one of the particles shown in Fig. 2A. The image 2B (and also the impression of the particles in image 2A) indicated that the shape of the particles was cubic in nature. TEM-determined size of the NPs was about 50 nm. Fig. 2C represents the SAED (selected area electron diffraction) pattern of the NP obtained from TEM study. The pattern with distinct spots spread over three complete concentric rings (one spot of each ring is marked by an arrow) indicated the crystallinity of the particle. The distances between crystal planes, called d-values, were determined from the mean distances between the center and every spot of each ring. With the help of the scale bar (2 nm^{-1}) in the SAED image, the d-values were measured to be 1.43, 2.01 and 2.73 Å, corresponding to the rings from higher to lower distances from the center. When these d-values were matched with the JCPDS data files, the file no. (05-0661) clearly demonstrated that the NPs were made of Cu(II) oxide with crystal planes (1 1 1), ($\bar{1}$ 1 1), (0 0 2) corresponding to the d-values 1.43, 2.01 and 2.73 Å, respectively. Existence of such crystal planes in CuO-NP were also reported elsewhere [6]. Therefore, the SAED result further confirmed that the building block molecule of our NPs was CuO, not Cu_2O.

3.1.2. Compositional analysis of CuO-NP and trace of metal oxide bond in the NPs

The electron dispersion spectrum and the corresponding elemental energy-mass data (Fig. 3A) demonstrated that the basic elemental composition of CuO-NP was copper (mass % = 8.68) and oxygen (mass % = 21.03); other three elements present in the experimental sample were chlorine (mass % = 10.12, a component of the precursor $CuCl_2$), sodium (mass % = 14.19, a component of the reducing agent sodium borohydride) and carbon (mass % = 45.97, a component of the stabilizing agent PVA). This result implied that almost 75% of the NP mass was due to copper oxide stabilized with PVA and the rest of the mass was due to chlorine and sodium contamination, originated from the NP-precursor $CuCl_2$ and the reducing agent $NaBH_4$. Fig. 3B and C represents the FTIR spectra of pure PVA and Cu(II) oxide NP respectively. In PVA spectrum (Fig. 3B), bands at 3419, 2920, 1729, 1645 and 1041 cm^{-1} signified stretching vibrations of O–H, C–H, C═O, C═C and C–O–C bonds respectively, bands at 1429 and 1374 cm^{-1} reflected bending and wagging of CH_2 vibration respectively, and bands at 1264 or 1220 cm^{-1} indicated C–H wagging of PVA. On the other hand, Fig. 3C shows that in CuO-NP, absorption bands of C═O, C═C and O–H increased slightly from 1729 to 1738 cm^{-1}, 1645 to 1655 cm^{-1} and 3419 to 3421 cm^{-1} respectively. Moreover, the peaks around 1,000–600 cm^{-1} in spectrum of the NP (Fig. 3C) were attributed to the metal–oxygen stretching of CuO [30] and particularly appearance of a new peak at ~605 cm^{-1} confirmed the presence of nano-sized CuO particles in PVA matrix. Thus, FTIR result indicated that CuO surface was modified by PVA because, vibrational frequency of some bonds in PVA were altered due to formation of CuO-NP.

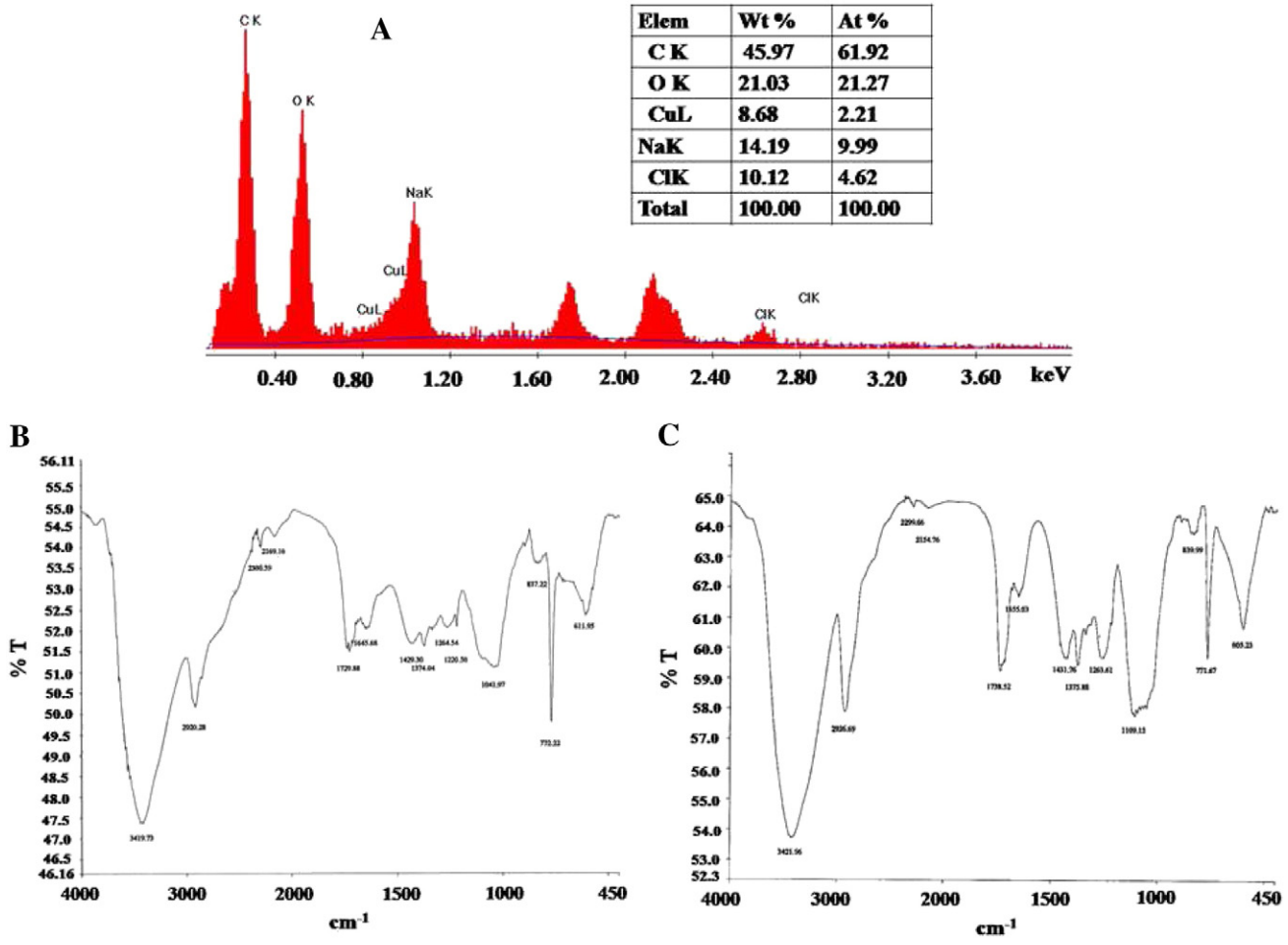

Fig. 3. Compositional analysis and trace of metal oxide bond in NPs. A) Electron dispersion spectrum with mass % of the constituents of CuO-NP; B) and C) represent FTIR spectra of PVA and CuO-NP respectively.

3.1.3. Semiconducting nature and band gap energies of the NP

Exponential nature of the current–voltage (I–V) characteristics in CuO-NP, as observed from the conductive-mode AFM result (Fig. 4A), indicated semi-conductive behavior of the NPs. The bulk CuO and CuO-NP both were reported to have semiconducting property; however, their band gap energy was different, being about 1.85 eV for bulk CuO [31] and 2.4–3.6 eV for CuO-NP [12,14,26,29]. Band gap energy of our particles was measured spectrophotometrically, using the Tauc's equation $\alpha(h\nu) = A(h\nu\text{-}E_g)^{m/2}$ as described in [32], where 'α' was absorption co-efficient of NP suspension, $h\nu$ (= hC/λ) was energy of incident light of wavelength λ, E_g was band gap energy, 'A' was a constant and 'm' depended on nature of transition (m = 1 for direct transition of electrons [33]). Putting m = 1, Tauc's equation became $(\alpha h\nu)^2 = A^2 (h\nu\text{–}E_g)$. Fig. 4B exhibits plot of $(\alpha h\nu)^2$ vs. $h\nu$, which has two slopes corresponding to the two extrapolated straight lines; the points of intersection of the extrapolations on X-axis denoted the values of E_g and these were 3.40 and 3.96 eV corresponding to the absorption peaks 370 and 266 nm respectively. These blue shifted values of E_g, compared to that of the bulk (1.85 eV) might be suggested to be due to quantum size effect [34].

3.1.4. Percentage of $CuCl_2$ converted to NPs

The NP suspension was centrifuged at 55,000 rpm for 25 min and the centrifuged pellet and supernatant were separately analyzed by AAS to determine their copper contents. The result, represented by Table 1, demonstrated that Cu^{++} concentrations in the pellet and supernatant of Cu(II) oxide NP suspension were about 80 and 20% respectively. This result clearly signified that 80% of the precursor $CuCl_2$ was converted to CuO-NPs. In parallel, control experiment was also carried out on $CuCl_2$ solution (of equivalent concentration present in NP suspension); no visible pellet was found and almost all the copper ions (95%) were present in the supernatant.

Different characteristics of the Cu(II) oxide NP, as determined here, have been put altogether in Table 2. It should be mentioned here that all the above characterization studies, except two — FTIR and AAS, were performed with the synthesized NP as a whole, without removing the unutilized $CuCl_2$.

3.2. Bacteriotoxicity of CuO-NP and mechanism of cell killing

3.2.1. MIC, MBC of CuO-NP for E. coli and S. aureus

The results of investigation on the antibacterial potency of the NP demonstrated that when the said bacterial cells were separately incubated overnight (18 h) in LB medium in the presence of different concentrations of the NP, the viable cell number increased over the pre-incubated initial cell number (6×10^6 per mL) for NP concentrations below 120 μg/mL (Table 3); however, the extent of increase decreased gradually with increase of NP concentration. At the concentration of 120 μg/mL of NPs in the growth medium, number of cells (7.5×10^6 per mL) after 18 h incubation remained nearly the same as that before incubation (6×10^6 per mL). Therefore, a bacteriostatic environment was created by the presence of 120 μg/mL CuO-NPs in the growth medium. Thus, the MIC of Cu(II) oxide NP for *E. coli* was 120 μg/mL. Table 3 also shows that above MIC, viable cell counts decreased gradually with increase of NP concentration. At a concentration of 160 μg/mL, cell number decreased by almost 99.9% (from 6×10^6 to 3.4×10^3 cells/mL), implying that the MBC of CuO-NPs in the case of *E. coli* was about 160 μg/mL. Results of two control experiments, where cells were incubated for 18 h with (i) PVA and $NaBH_4$ together and (ii) $CuCl_2$ alone, at concentrations present in 160 μg/mL NP (the MBC), showed that neither of the ingredients had any bactericidal effect on *E. coli*. However, at much larger concentration of $CuCl_2$, there was growth inhibitory (MIC at 236 μg/mL) and cell killing (MBC at 472 μg/mL) effects [4,35]. Similarly, for Gram positive bacteria *S. aureus* also, the NPs showed antibacterial effect with MIC and MBC as 180 and 195 μg/mL respectively (Table 3). For *S. aureus*, higher values of MIC and MBC than the corresponding values for *E. coli* seemed to be due to thicker peptidoglycan layer of Gram positive cells. Regarding antibacterial potency of CuO-NP on *E. coli*, one group reported the MBC of their synthesized particle was 250 μg/mL [7]; another one reported that 90% cell killing occurred by their CuO-NP at 900 μg/mL [6]; a recent report by a group demonstrated that 1000 μg/mL of their synthesized CuO-NP inhibited *E. coli* growth after 9 h [2]. For *S. aureus*, reported values of antibacterial concentration of differently synthesized CuO-NPs were 2500 μg/mL [7] and 1000 μg/mL [2]. All these reports indicated that the CuO-NP synthesized by our method had high antibacterial potency.

Table 1
AAS result for CuO-NP suspension and $CuCl_2$ solution, each diluted to 1 mM (63.5 mg/L) of copper.

Sample	Raw (mg/L)	Pellet (mg/L)	Supernatant (mg/L)
CuO-NPs	61.87	50.47	11.671
$CuCl_2$	62.7	3.12	59.89

3.2.2. Generation of ROS and its consequences in NP-treated E. coli cells

To understand the mechanism of bacterial killing by Cu(II) oxide NP, first we investigated whether there was any generation of reactive oxygen species (ROS) in NP-exposed cells; because, nanoparticles of other metal oxides like TiO_2, ZnO, MgO caused *E. coli* cell death through

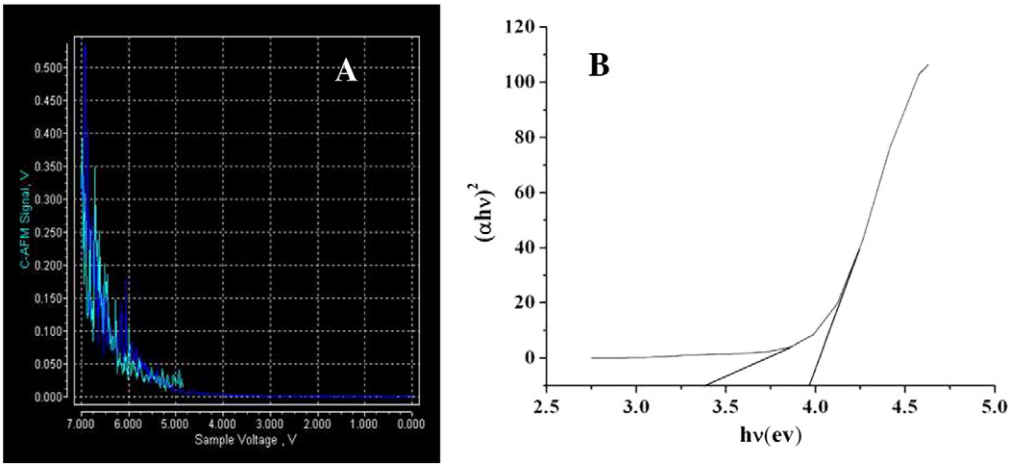

Fig. 4. Determination of semiconducting nature and band gap energies of NPs. A) Current–voltage characteristics of CuO-NP, as measured by C-AFM; B) the plot of Tauc's equation.

Table 2
Important characteristics of the Cu(II) oxide NP.

Color	Optical property	Size measured by			Shape	Crystal planes	Electric property	% of precursor converted to the NP
		DLS	AFM	TEM				
Deep green	Absorption maxima at 266 and 370 nm	(80 ± 20) nm	70 nm	50 nm	Cubic	(1 1 1), ($\bar{1}$ 1 1), (0 0 2)	Semi-conductive with band gaps of 3.40 and 3.96 eV	80

induction of ROS viz., superoxide anion ($O_2^{\bullet}$), hydroxyl radical ($^{\bullet}OH$) and singlet oxygen ($^1O_2$) [36]. So far Cu(II) oxide NP-mediated production of ROS is concerned, there were contradictory reports; some showed evidence in favor of ROS generation [3,6], whereas some showed no induction of ROS [36] in *E. coli* by CuO-NP. However, through flow cytometry study, we found significant generation of ROS in *E. coli*, when the cells were allowed to grow overnight (18 h) in the presence of sub-MIC level of NP (90 μg/mL). The result of flow cytometry experiment was illustrated using dot plots (Fig. 5 A–C). The dots in the lower left (LL) region of Fig. 5 represented cells with basal level ROS, whereas those shifted from LL to LR (lower right) and UR (upper right) regions implied cell population with enhanced ROS level. Therefore, Fig. 5A represents that in normal/control population of *E. coli*, most of the cells (95.43%) contained basal level ROS. Fig. 5B shows that for cells treated with 90 μg/mL of CuO-NP, 75.1% (LR: 56.31 + UR: 18.79) of the cells had enhanced ROS level, demonstrating clearly the NP-mediated generation of ROS in *E. coli* cells. The precursor $CuCl_2$ (90 μg/mL) also generated ROS, however, extent of generation was much less, because only 37.49% cells were shifted to LR (18.92%) and UR (18.57%) regions (Fig. 5C). Moreover, when the mean fluorescence intensity was plotted against concentration, the plot (Fig. 5D) exhibited that the extent of fluorescence intensity or in other words the amount of ROS generation in NP-treated cells was more than double of that in the equivalent amount of $CuCl_2$-treated cells, which was further about 3 times more than basal level ROS in control cells (treated with nothing). It should be mentioned here that control experiment was also performed with cells exposed to 10 mM H_2O_2 for 1 h; the result of which showed pronounced level of ROS generation in the treated cells compared to the untreated control cells (result shown as Supplementary material). Gunawan et al. [6] showed that Cu-nitrate or CuO-NP, each at a concentration of 365 ppm, caused equal amounts of a) ROS generation and b) cell killing after 6 h of incubation. However, our results demonstrated that in CuO-NP-exposed cells, compared to the equivalent amount of $CuCl_2$-exposed cells, more ROS was generated and so, more cell killing occurred; this was supported by the observations of Applerot et al. [3].

ROS were known to kill cells due to either or all of the reasons like lipid per-oxidation, protein oxidation and chromosomal DNA degradation [37,38]. Our results also demonstrated that exposure of *E. coli* cells to 90 and 120 μg/mL CuO-NP for 18 h increased cellular lipid per-oxidation level by about 38- and 45-folds respectively, compared to that in untreated control cells (Fig. 6A). On the other hand, cellular exposition to bulk copper salt (120 μg/mL of $CuCl_2$) caused much less increase in lipid per-oxidation by only 15-folds. This lipid per-oxidation i.e., the oxidation of unsaturated fatty acids in *E. coli* membranes was a probable initiating event for bacterial killing by CuO-NP, because changes in fatty acid composition perhaps altered physical properties of lipid bi-layer, affecting membrane fluidity and activity of integral membrane proteins. When experiment was carried out, as described in [1], to investigate whether there was any oxidation of proteins by the generating ROS in the NP-exposed cells, no remarkable effect was observed (data not shown). Fig. 6B exhibits that there was degradation of chromosomal DNA in *E. coli* cells exposed to both 120 and 135 μg/mL NP. The intensity of the bands clearly shows that the DNA degradation in 135 μg/mL NP-treated cells (lane d) was higher than that in 120 μg/mL NP-treated cells (lane a). Treatment of cells with 135 μg/mL $CuCl_2$ also caused some degradation (as observed from low band intensity in lane b compared to that in lane c); however, extent of DNA degradation in cells exposed to the NP was significantly high (comparing intensity of the bands in lanes a and d with lane c). Low intensity of DNA bands of NP-treated cells compared to that of untreated cells signified DNA degradation and migration of many small degraded fragments out of the gel during electrophoresis.

Table 3
Number of viable cells, after 18 h incubation in the presence of the increasing concentrations of CuO-NP. Initial numbers of cells, before incubation, were 6×10^6 cells/mL for *E. coli* & 3×10^6 cells/mL for *S. aureus*.

CuO-NP in (μg/mL)	No. of viable *E. coli* cells	CuO-NP in (μg/mL)	No. of viable *S. aureus* cells
0	5.8×10^9	0	4.1×10^9
60	4.5×10^9	90	3.2×10^9
90	2.1×10^8	150	1.4×10^8
120 (MIC)	7.5×10^6	180 (MIC)	3.8×10^6
135	4.0×10^4	190	2.6×10^4
160 (MBC)	3.4×10^3	195 (MBC)	1.8×10^3

3.3. Modification of CuO-NPs by bacterial growth medium

3.3.1. Interaction of CuO-NPs with media organics and amino acids

In order to understand the mechanism of action of CuO-NP, we investigated the state of the NPs in bacterial growth medium LB. Fig. 7A shows that the addition of CuO-NP in LB generated absorption maxima at 616 nm, where the intensity increased with stepwise addition of NPs (at steps of 30 μg/mL) up to 180 μg/mL. On the other hand, addition of $CuCl_2$ in LB medium also exhibited absorption maxima, however, stepwise addition of $CuCl_2$ by 30 μg/mL (up to 180 μg/mL) caused gradual increase of intensity with shift of absorption peak from 606 nm to 636 nm (Fig. 7B). It should be mentioned here that 1) by the gradual addition of NPs in water only, a very little absorbance with very flattened peak at 630 nm appeared (Supplementary Fig. 2); however, quite altered nature of the spectra at lower wavelength (~450 nm) region with no point of contact, unlike the nature in LB, was possibly due to some scattering effect and 2) by the stepwise addition of $CuCl_2$ in water, no absorbance was found to appear in the wavelength region at 400–800 nm (result not shown). Since, LB itself had no characteristic absorption peak, Fig. 7A therefore implied that some complex formation occurred between NPs and the components of LB medium. However, comparison of Fig. 7A and B signified that the nature of the interacting product between Cu(II) oxide NP and LB components was quite different from that between $CuCl_2$ and LB components; moreover, in the case of $CuCl_2$, the nature of the interacting product varied continually (as the absorption peak gradually red-shifted) with increasing addition of salt. This was because the pH (7.4) of the LB medium did not change by addition of NPs (up to 180 μg/mL) of physiological pH, but the LB pH became gradually acidic with stepwise addition of $CuCl_2$ and drastically came down to about 5.5 by addition of 180 μg/mL $CuCl_2$ (Fig. 7C). So, the free copper ion concentration (if any) in the NP-containing LB medium was negligible compared to its high concentration present in the $CuCl_2$ (equivalent amount of the NP)-containing LB. Thus, the higher antibacterial activity of CuO-NP than its precursor $CuCl_2$, as observed from our results on the MIC and MBC, was suggested to be a 'particle-specific effect' rather than an 'ion-specific effect'. In case of $CuCl_2$, cell killing might be caused by

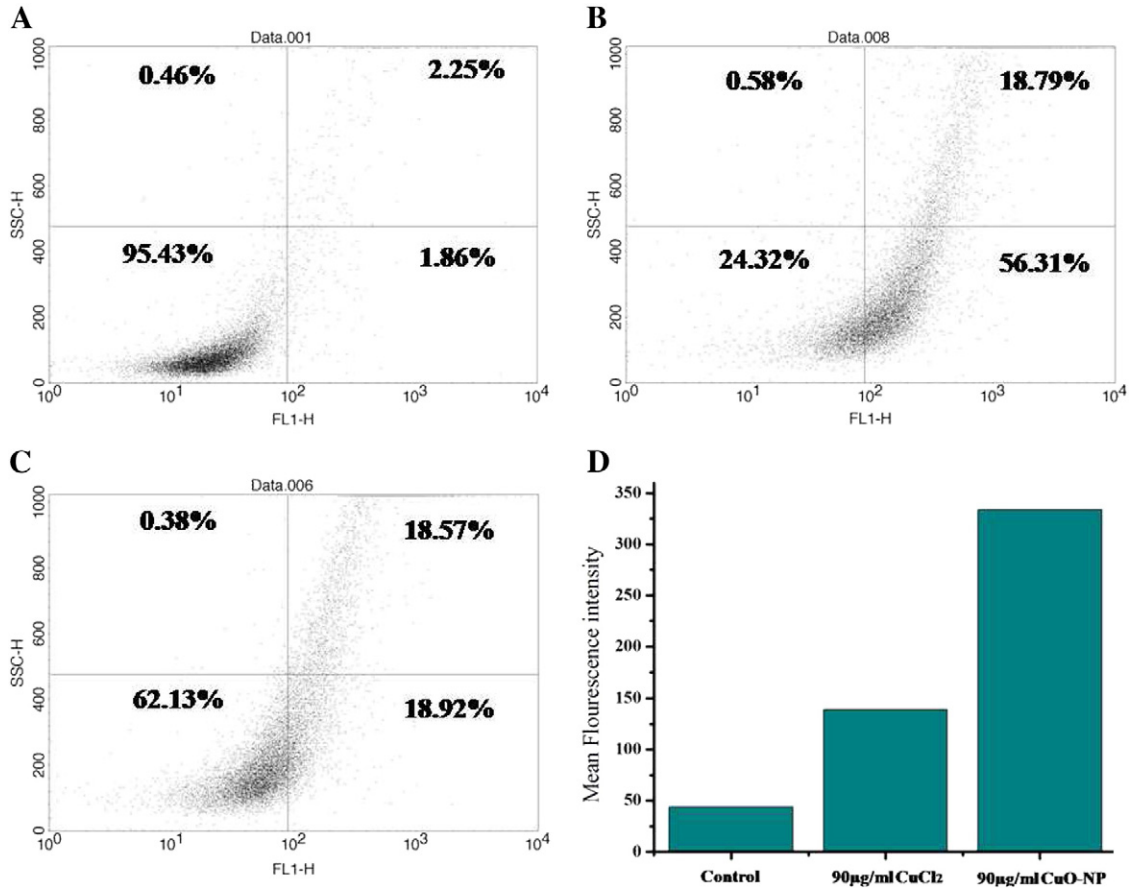

Fig. 5. Flow cytometric analysis of ROS generation in *E. coli* cells. A) Untreated control, B) Cells treated with 90 μg/mL CuO-NP, C) Cells treated with 90 μg/mL $CuCl_2$, D) measure of DCF mean fluorescence intensity.

considerable lowering of media pH and/or by some Cu-complex formed in the growth medium, whereas in case of CuO-NP, the complex between NP and LB components directly killed the cells. LB, being a complex undefined medium having yeast extract, bactotryptone etc., contains pool of organic substances like amino acids, nucleotides, vitamins etc. Therefore, it seemed that the NP interacted with these media organics. In order to investigate whether there was really any interaction of the NP with free amino acids, in vitro UV–Vis spectrophotometric study was performed. The results showed that with addition of different amino acids (Lys, Glu, Ser, and Gly) separately and mixture of twenty different L-amino acids at increasing concentrations (0, 10, 25, 50, 75, 100, 200 and 500 μg/mL) to CuO-NP suspension (360 μg/mL),

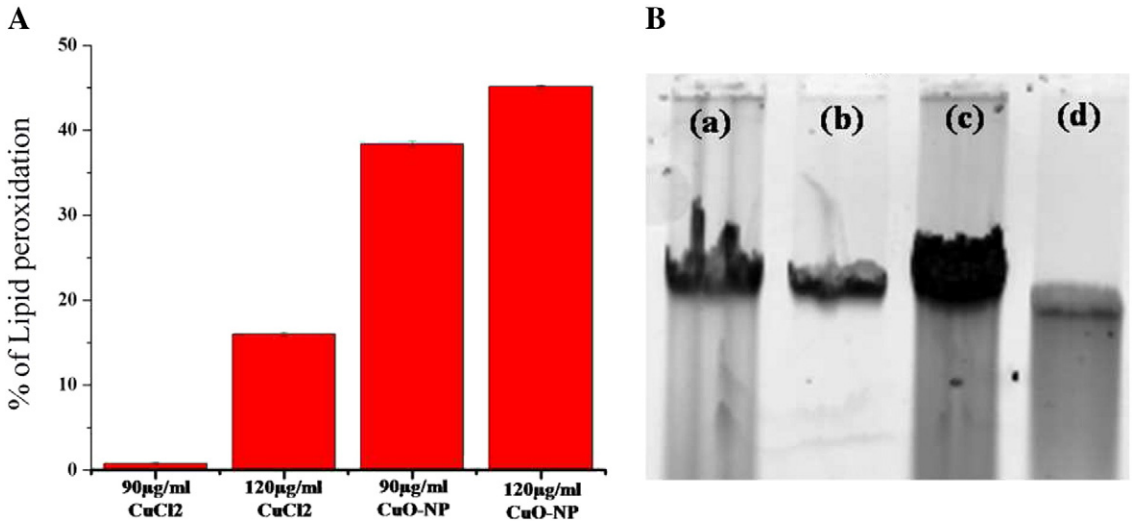

Fig. 6. A) Lipid peroxidation and B) chromosomal DNA degradation in the NP-treated *E. coli* cells. In panel B, lane a: cells treated with 120 μg/mL CuO-NP, lane b: cells treated with 135 μg/mL $CuCl_2$, lane c: control cells (untreated one) and lane d: cells treated with 135 μg/mL CuO-NP. DNA was isolated from cells of the four samples, after equalizing their optical densities at 600 nm to make the cell number of each sample equal.

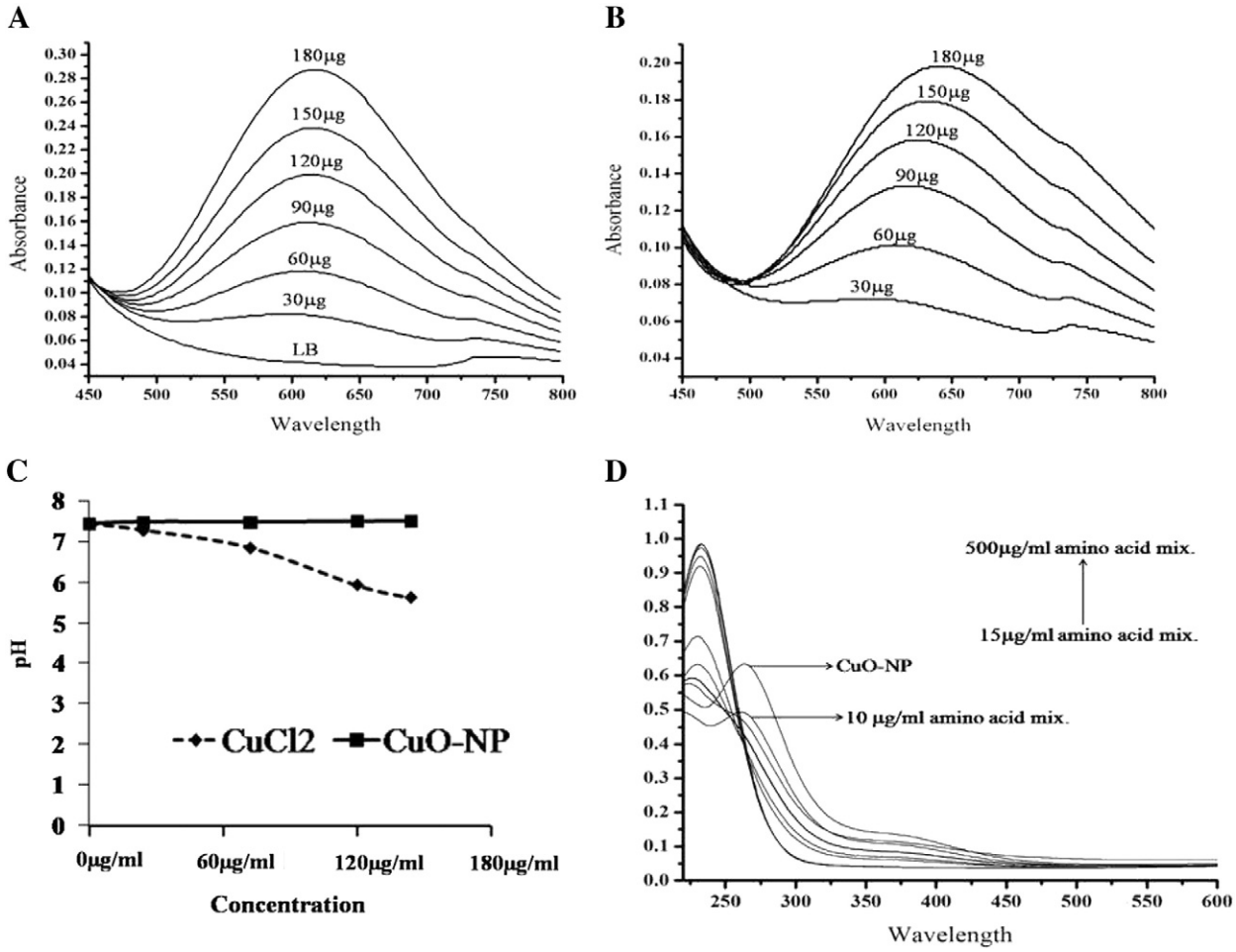

Fig. 7. Interaction of media organics/amino acids mix with CuO-NP/Cu ions. Changes in absorption spectrum of A) LB medium with stepwise addition of CuO-NPs, B) LB with stepwise addition of $CuCl_2$, C) Changes in the pH of LB media with stepwise addition of $CuCl_2$ and CuO-NP separately and D) Changes in absorption spectrum of NP suspension with stepwise addition of amino acid mixture.

the absorption peak of the NP at 370 nm gradually decreased and finally abolished, whereas the peak at 266 nm first decreased and then blue-shifted to the wavelength range at 230–235 nm (Fig. 7D, where only the result of amino acids mixture has been shown); at the blue-shifted wavelength, the intensity further increased with the gradual addition of any amino acid or amino acids mix. Our result of blue-shifting of the NP absorption peak (from 266 nm to 230–235 nm) by the addition of amino acids mix conformed well with that of El-trass et al. [39], where the absorption peak of their synthesized CuO-NP at 290 nm shifted to 240 nm by the addition of the amino acids. This result clearly demonstrated that CuO-NP interacted with amino acids forming some complex. Moreover, when the amino acid mix was made more complex by adding nucleotide mix, vitamins A and B (all in the proportions present in MOPS medium [19]), and the whole mixture was added to the NP suspension, absorbance at the 230–235 nm region shifted to the range of 600 nm (data not shown), which was close to the absorbance of the NP-contained LB. It should be mentioned here that the stepwise addition of pre-formed NP-amino acids complex in LB medium also showed a gradual increase of absorbance at 616 nm (data not shown), as was observed with gradual addition of the NP alone in LB. Thus, results of all the spectrophotometric studies, described in this subsection, indicated clearly that NPs got modified with media organics.

3.3.2. Nature of the modified CuO-NPs

NPs-amino acids interaction was further confirmed by DLS experiment. When the amino acid lysine (500 μg/mL) was allowed to interact with CuO-NP (360 μg/mL) for 15 min, the mixture had two distinct size distribution peaks corresponding to the particles of average sizes around 240 and 20 nm (Fig. 8A1) with the percentage of particle numbers as 30 and 70%, respectively. Instead, free NPs had a single size distribution peak around 80 nm of 100% population (Fig. 1B). Therefore, 240 nm-sized particle seemed to be the size of NP-lysine complex, which was about three times larger than free NP. When PVA, the stabilizing agent of CuO-NP, was stirred and studied by DLS instrument, two peaks appeared — one for particles of size 30 nm covering 92% of population and the other for particles of size 3000 nm covering 8% of the population (Fig. 8A2). The majority particles of size 30 nm were surely of normal PVA aggregates, whereas the negligible (8%) presence of larger particles might be due to some large aggregates of PVA or due to any contaminant. Comparison of Figs A1 and A2 suggested that during interaction between NP and lysine, PVA was released from NPs and the free hydrophobic PVA molecules agglomerated to form particles of size about 20 nm in the aqueous environment of lysine-bound NPs. Release of PVA did not destabilize the NPs because, lysine also had good stabilizing property. Since, the hydrodynamic size of NPs (about 80 nm) was much larger than that of PVA aggregates (about 20 nm), it might be expected that the released PVA molecules from one NP surface produced a number of PVA assemblies and thereby made the number ratio of particles of PVA-aggregates to modified CuO-NP (i.e., NP-lysine complex) as 70:30.

The above proposition of NP-lysine interaction with the release of PVA was further supported by the results of our XPS study. To understand the evolution of metal-ion bonds in CuO-NP as well as in

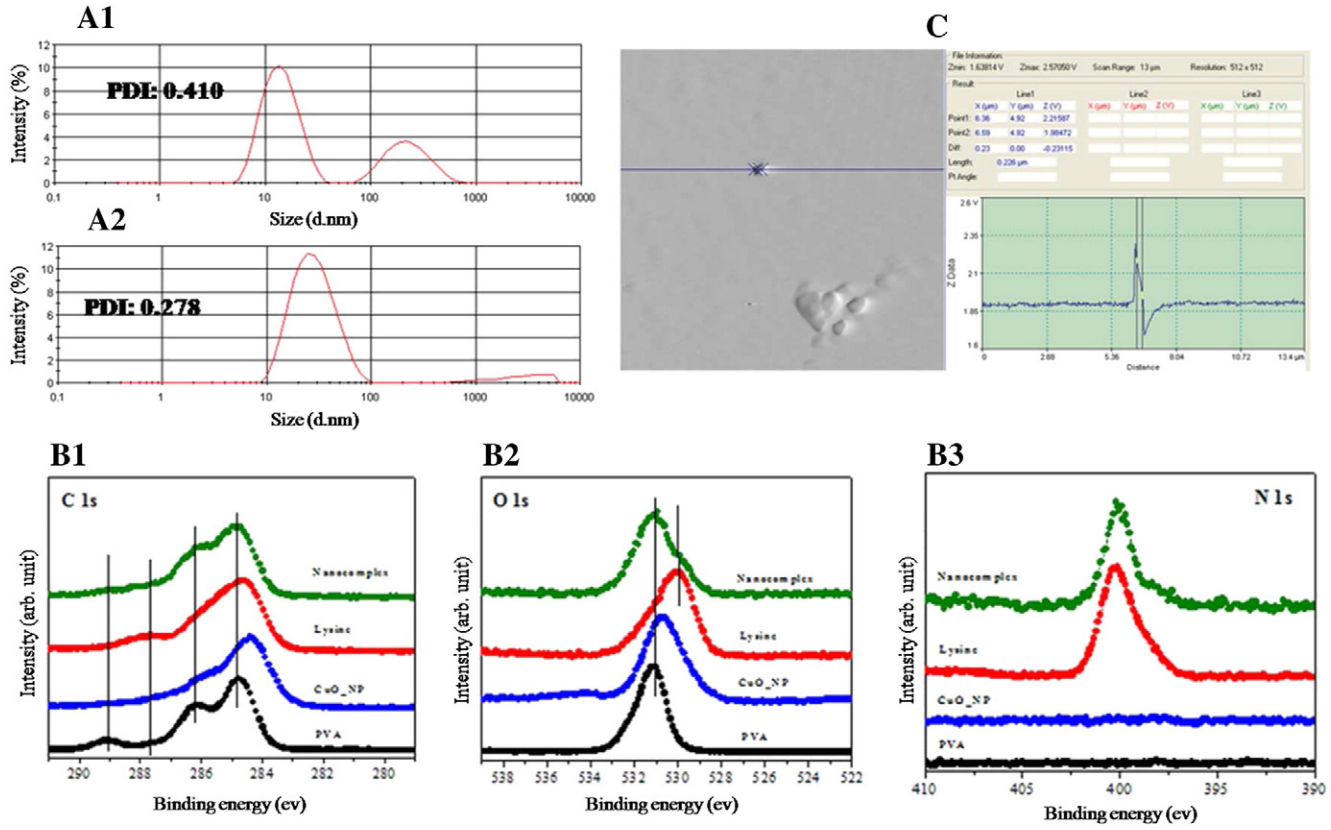

Fig. 8. Modification of CuO-NP by lysine. A1: Size distribution pattern of NPs after interaction with lysine, A2: size distribution pattern of stirred PVA only, B1, B2, and B3: C 1 s, O 1 s and N 1 s core level spectra of CuO-NP, modified CuO-NP (i.e. CuO-NP-lysine nanocomplex), lysine and PVA alone. C: AFM image of modified CuO-NP and scanned parameters of the modified particles marked by an arrow.

CuO-NP-lysine nanocomplex, detailed core level photoemission measurements were done on these systems along with pure PVA and lysine as reference samples. Acquired spectra from the C 1 s, O 1 s and N 1 s core levels for all the four cases are presented in Fig. 8B. C 1 s spectrum of the pure PVA system, shown in Fig. 8B1, was composed of four peaks appearing at around 284.2, 286.1, 287.6 and 288.8 eV binding energy positions corresponding to the hydrocarbon bonds (C – C/C – H), methylene carbon singly bonded to oxygen (C – O/C – OH), carbonyl bond (C═O) and the ester carbon bonds (O – C═O/COOCH3), respectively [40,41]; whereas that of the free lysine was primarily composed of peaks around 284.6 and 287.7 eV corresponding to the energies of C – H and C═O functional groups respectively, observed in polymers [42]. From the C 1 s spectrum of CuO-NP, one can clearly observe the modifications in the spectral shape as well as the binding energy position of C peaks, suggesting the modification/formation of C-bonds in the PVA-stabilized NP. C 1 s spectrum of NP-lysine complex exhibits PVA type spectral features, suggesting release out of PVA from the NP with the formation of nanocomplex. Fig. 8B2 and B3 show respectively the O 1 s and N 1 s spectral features acquired from the same set of samples, which corroborated the results represented by C 1 s spectra. O 1 s spectrum of free PVA was primarily composed of peak appearing at around 531.0 eV binding energy where as that of free lysine was composed of main peak appearing at around 530.0 eV, as expected [41,42]. O 1 s spectrum of CuO-NP shows shift in binding energy positions and modification of spectral shape from that of the PVA, indicating appearance of some new bond in PVA-stabilized NP; whereas that of the nano-complex shows main peak at 531 eV corresponding to the binding energy position of PVA and a shoulder appearing at 530.0 eV corresponding to the peak position of lysine, possibly arising from a bond formation between NP and lysine. In the case of N 1 s spectra, there is complete absence of N peaks in the cases of PVA and CuO-NP, as expected. On the other hand, the spectrum of lysine is found to be composed of two peaks appearing at around 400.2 and 398.0 eV [42]; upon complex formation, the spectral intensity of the lower binding energy peak is suppressed significantly, implying once more the possibility of arising some bond between CuO-NP and lysine in the nanocomplex. Thus, the XPS results corroborated our DLS findings on the formation of some complex between CuO-NP and lysine with simultaneous removal of the stabilizer PVA from the NPs.

Moreover, when the NP-lysine mixture was visualized through AFM, the image displayed particles of size about 220–240 nm (Fig. 8C). No particle of size around 20–30 nm (PVA agglomerate) was observed in the field of view; perhaps, this was because the force field of larger modified NP hindered the AFM cantilever to come down up to the smaller PVA agglomerate particle. Therefore, our findings led us to propose the mechanism of antibacterial role of CuO-NP as follows: on addition of CuO-NPs to growing bacterial cells, organic components in growth medium had bound on NP surface displacing the stabilizer PVA and changing the original CuO-NP to some modified nanoform, which produced ROS in bacterial cells causing cytotoxicity through lipid per-oxidation and DNA degradation. This proposition has been pictorially presented in Fig. 9.

4. Conclusion

In this communication a simple, fast, economic and robust method of synthesis of highly stable colloidal CuO-NPs of physiological pH has been described. It was a reduction–oxidation method using $CuCl_2$ as precursor molecule, $NaBH_4$ as reducing agent and PVA as stabilizer. In our method, about 80% of $CuCl_2$ was converted to NPs, which were about 50 nm in size, cubic in shape, had semiconducting property and remained stable over 3 months. Antibacterial activity of our particles was much higher than that of the CuO-NPs prepared by other methods. Origin of antibacterial property, with respect to *E. coli*, was due to

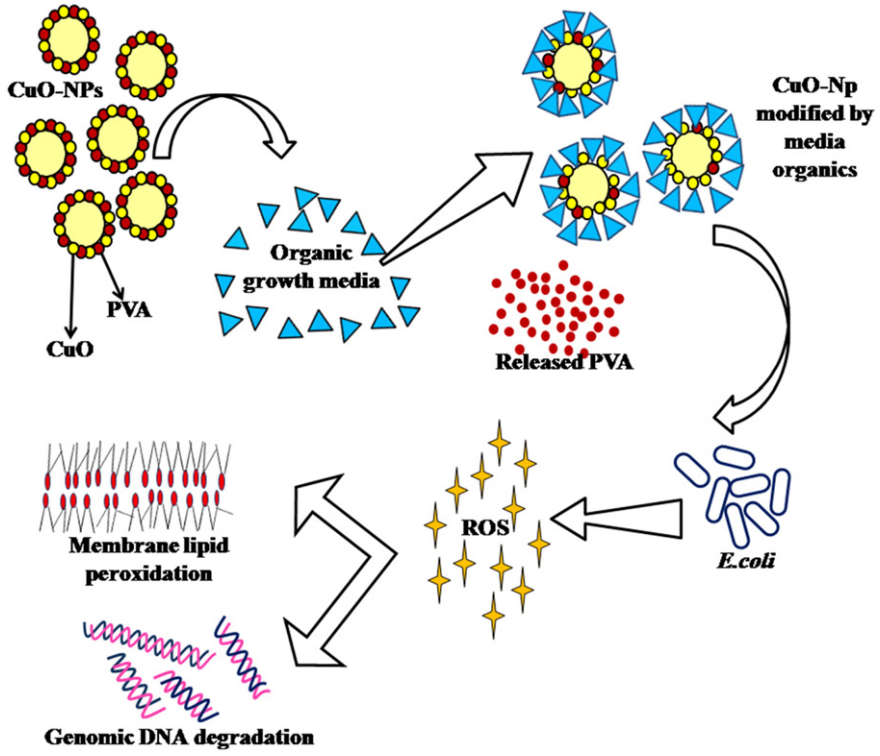

Fig. 9. A schematic representation of the proposed mode of action of CuO-NPs.

generation of ROS, which caused cell membrane damage through lipid per-oxidation and cellular DNA damage through phospho-di-ester bonds breakage. Our results signified that antibacterial role of the NP was a 'particle-specific effect', not an 'ion specific effect' (i.e., due to leaching of Cu-ions from the NP surface). Our findings further demonstrated that the NPs were modified by the organic components of cell growth medium and in the process of modification, the stabilizing agent PVA of the NPs was exchanged by media organics with consequent increase of NP size; saturating concentration of the organic components in growth medium increased the size of CuO-NPs to about three times of their normal size. We suggest that the modified NPs caused generation of ROS in growing bacterial cells.

From the application aspect of the present study, it can be said that in the future, our CuO-NP may have potential use as an antibacterial agent; further in vitro studies on cell lines and in vivo studies on animal system may help to develop a potent drug out of this CuO-NP, to substitute antibiotics.

Transparency document

The Transparency document associated with this article can be found, in the online version.

Acknowledgments

We are indebted to a) DBT, GOI (BT/PR11477/NNT/28/416/2008) for the financial assistance; b) DST, GOI for supporting the first author with INSPIRE FELLOWSHIP, its 'FIST Programmes — 2001–12' of our department, and its 'PURSE Programme — 2012–15' of the university and c) UGC, GOI for its 'SAP Programme — 2011–16' of our department for providing different instrumental and infrastructural support.

Appendix A. Supplementary data

Supplementary data to this article can be found online at http://dx.doi.org/10.1016/j.bbagen.2015.01.015.

References

[1] A.K. Chatterjee, R. Chakraborty, T. Basu, Mechanism of antibacterial activity of copper nanoparticle, Nanotechnology 25 (2014). http://dx.doi.org/10.1088/0957-4484/25/13/135101.
[2] D. Das, B.C. Nath, P. Phukon, S.K. Doluia, Synthesis and evaluation of antioxidant and antibacterial behavior of CuO nanoparticles, Colloids Surf. B: Biointerfaces 101 (2013) 430–433.
[3] G. Applerot, J. Lellouche, A. Lipovsky, Y. Nitzan, R. Lubart, A. Gedanken, E. Banin, Understanding the antibacterial mechanism of CuO nanoparticles: revealing the route of induced oxidative stress, Small 8 (2012) 3326–3337.
[4] A.K. Chatterjee, R.K. Sarkar, A.P. Chattopadyay, P. Aich, R. Chakraborty, T. Basu, A simple robust method for synthesis of metallic copper nanoparticles of high antibacterial potency against *E. coli*, Nanotechnology 23 (2012) (085103 pp11).
[5] P. Pandey, S. Merwyn, G.S. Agarwal, B.K. Tripathi, S.C. Pant, Electrochemical synthesis of multi-armed CuO nanoparticles and their remarkable bactericidal potential against waterborne bacteria, J. Nanoparticle Res. 14 (2012). http://dx.doi.org/10.1007/s11051-011-0709-0.
[6] C. Gunawan, W.Y. Teoh, C.P. Marquis, R. Amal, Cytotoxic origin of copper(II) oxide nanoparticles: comparative studies with micron-sized particles, leachate, and metal salts, ACS Nano 9 (2011) 7214–7225.
[7] G. Ren, D. Hu, E.W.C. Cheng, M.A. Vargas-Reus, P. Reip, R.P. Allaker, Characterisation of copper oxide nanoparticles for antimicrobial applications, Int. J. Antimicrob. Agents 33 (2009) 587–590.
[8] J.P. Ruparelia, A.K. Chatterjee, S.P. Duttagupta, S. Mukherji, Strain specificity in antimicrobial activity of silver and copper nanoparticles, Acta Biomater. 4 (2008) 707–716.
[9] J.F. Xu, W. Ji, Z.X. Shen, S.H. Tang, X.R. Ye, D.Z. Jia, X.Q. Xin, Preparation and characterization of CuO nanocrystals, J. Solid State Chem. 147 (2009) 516–519.
[10] B. Kavita, J.B. Singh, M.V. Rama Rao, T. Shripathi, S. Mahamuni, Quantum size effects in CuO nanoparticles, Phys. Rev. B 61 (2000) 11093–11096.
[11] R.V. Kumar, Y. Diamant, A. Gedanken, Sonochemical synthesis and characterization of nanometer-size transition metal oxides from metal acetates, Chem. Mater. 12 (2000) 2301–2305.
[12] H. Wang, J.Z. Xu, J.J. Zhu, H.Y. Chen, Preparation of CuO nanoparticles by microwave irradiation, J. Cryst. Growth 244 (2002) 88–94.
[13] A.A. Eliseev, A.V. Lukashin, A.A. Vertegel, L.I. Heifets, A.I. Zhirov, Y.D. Tretyakov, Complexes of Cu(II) with polyvinyl alcohol as precursors for the preparation of CuO/SiO2 nanocomposites, Mater. Res. Innov. 3 (2000) 308–312.
[14] D.I. Son, C.H. You, T.W. Kim, Structural, optical, and electronic properties of colloidal CuO nanoparticles formed by using a colloid-thermal synthesis process, Appl. Surf. Sci. 255 (2009) 8794–8797.
[15] S. Dagher, Y. Haik, I.A. Ayesh, N. Tit, Synthesis and optical properties of colloidal CuO nanoparticles, J. Lumin. 151 (2014) 149–154.
[16] M. Banik, T. Basu, Calcium phosphate nanoparticles: a study of their synthesis, characterization and mode of interaction with salmon testis DNA, Dalton Trans. 43 (2014) 3244–3259.

[17] D.R. Janero, Malondialdehyde and thiobarbituric acid-reactivity as diagnostic indices of lipid peroxidation and peroxidative tissue injury, Free Radic. Biol. Med. 9 (1990) 515–540.
[18] M.M. Bradford, A rapid and sensitive method for quantitation of microgram quantities of protein utilizing the principle of protein dye-binding, Anal. Biochem. 72 (1976) 248–254.
[19] K. Wilson, Preparations of genomic DNA from bacteria Current Protocols in Molecular Biology, Preparation and Analysis of DNA ed D D Moore, Wiley Interscience, New York, 1994. 2.4.1–2.4.5.
[20] J. Sambrook, D.W. Rusell, Molecular cloning: a laboratory manual, 3rd edn Cold Spring Harbor Laboratory Press, New York, 2001. 5.10–5.13.
[21] R.A. VanBogelen, F.C. Neidhardt, Preparation of *Escherichia coli* samples for 2-D gel analysis, in: J.L. Andrew (Ed.), 2-D Proteome Analysis Protocols: *Meth. In Mol. Biol*, Humana Press Inc., New Jersey, 1999, pp. 21–29.
[22] U. Manju, M. Sreemany, A.K. Chakraborty, Multi-technique photoelectron spectrometer for micro-area spectroscopy and imaging, Curr. Sci. 105 (2013) 1056–1060.
[23] M.N.K. Chowdhury, M.D.H. Beg, M.R. Khan, M.F. Mina, Synthesis of copper nanoparticles and their antimicrobial performances in natural fibres, Mater. Lett. 98 (2013) 26–29.
[24] Y. Bai, T. Yang, Q. Gu, G. Cheng, R. Zheng, Shape control mechanism of cuprous oxide nanoparticles in aqueous colloidal solutions, Powder Technol. 227 (2012) 35–42.
[25] U.S. Shenoy, A.N. Shetty, A facile one step solution route to synthesize cuprous oxide nanofluid, Nanosci. Nanotechnol. 3 (2013) (Art.5:2013).
[26] Y. Yu, J. Zhang, Solution-phase synthesis of rose-like CuO, Mater. Lett. 63 (2009) 1840–1843.
[27] X.Y. Chen, H. Cui, P. Liu, G.W. Yang, Shape-induced ultraviolet absorption of CuO shuttlelike nanoparticles, Appl. Phys. Lett. 90 (2007). http://dx.doi.org/10.1063/1.2736285.
[28] O. Bondarenko, A. Ivask, A. Käkinen, A. Kahru, Sub-toxic effects of CuO nanoparticles on bacteria: kinetics, role of Cu ions and possible mechanisms of action, Environ. Pollut. 169 (2012) 81–89.
[29] A.S. Lanje, S.J. Sharma, R.B. Pode, R.S. Ningthoujam, Synthesis and optical characterization of copper oxide nanoparticles, Adv. Appl. Sci. Res. 1 (2010) 36–40.
[30] S. Gandhi, H. Hari, R. Subramani, T. Ramakrishnan, A. Sivabalan, V. Dhanalakshmi, M.R. Gopinathan Nair, R. Anbarasan, Ultrasound assisted one pot synthesis of nano-sized CuO and its nanocomposite with poly(vinyl alcohol), J. Mater. Sci. 45 (2010) 1688–1694.
[31] K. Santra, C.K. Sarkar, M.K. Mukherjee, B. Gosh, Copper oxide thin films grown by plasma evaporation method, Thin Solid Films 213 (1992) 226–229.
[32] J. Morales, L. Sa'nchez, F. Martı'n, J.R. Ramos-Barrado, M. Sa'nchez, Use of low-temperature nanostructured CuO thin films deposited by spray-pyrolysis in lithium cells, Thin Solid Films 474 (2005) 133–140.
[33] M. Kaur, K.P. Muthe, S.K. Despande, S. Choudhury, J.B. Singh, N. Verma, S.K. Gupta, J.V. Yakhmi, Growth and branching of CuO nanowires by thermal oxidation of copper, J. Cryst. Growth 289 (2006) 670–675.
[34] Y. Liu, Y. Chu, Y.J. Zhuo, M.Y. Li, L.L. Li, L.H. Dong, Anion-controlled construction of CuO honeycombs and flowerlike assemblies on copper foils, Cryst. Growth Des. 7 (2007) 467–470.
[35] W.L. Du, Y.L. Xu, Z.R. Xu, C.L. Fan, Preparation, characterization and antibacterial properties against *E. coli* K88 of chitosan nanoparticle loaded copper ions, Nanotechnology 19 (2008). http://dx.doi.org/10.1088/0957-4484/19/8/085707.
[36] Y. Li, W. Zhang, J. Niu, Y. Chen, Mechanism of photogenerated reactive oxygen species and correlation with the antibacterial properties of engineered metal-oxide nanoparticles, ACS Nano 6 (2012) 5164–5173.
[37] J. Du, J.M. Gebicki, Proteins are major initial cell targets of hydroxyl free radicals, Int. J. Biochem. Cell Biol. 36 (2004) 2334–2343.
[38] R. Bakalova, H. Ohba, Z. Zhelev, M. Ishikawa, Y. Baba, Quantum dots as photosensitizers? Nature 22 (2004) 1360–1361.
[39] A. El-Trass, H. ElShamy, I. El-Mehasseb, M. El-Kemary, CuO nanoparticles: synthesis, characterization, optical properties and interaction with amino acids, Appl. Surf. Sci. 258 (2012) 2997–3001.
[40] A. Rogojanu, E. Rusu, N. Olaru, M. Dobromir, D.O. Dorohoi, Development and characterization of poly(vinyl alcohol) matrix for drug release, Dig. J. Nanomater. Bios. 6 (2011) 809–818.
[41] C. Inoue, Y. Kaneda, M. Aida, K. Endo, Simulation of XPS of poly(vinyl alcohol), poly(acrylic acid), poly(vinyl acetate), and poly(methyl methacrylate) polymers by an ab initio mo method using the model molecules, Polym. J. 27 (1995) 300–309.
[42] M.J. Bozack, Y. Zhou, S.D. Worley, Structural modifications in the amino-acid lysine induced by soft-X-ray irradiation, J. Chem. Phys. 100 (1994) 8392–8398.